

# Ground-state and thermal entanglements in non-Hermitian XY system with real and imaginary magnetic fields

Yue Li<sup>1</sup>, Pan-Pan Zhang<sup>1,2</sup>, Li-Zhen Hu<sup>1,2</sup>, Yu-Liang Xu<sup>1</sup> and Xiang-Mu Kong<sup>1\*</sup>

<sup>1</sup>*School of Physics and Optoelectronic Engineering,*

*Institute of Theoretical Physics, Ludong University, Yantai 264025, China and*

<sup>2</sup>*Department of physics, Beijing Normal University, Beijing 100875, China*

(Dated: April 21, 2023)

## Abstract

In this manuscript, we study the non-Hermitian spin-1/2 XY model in the presence of the alternating, imaginary and transverse magnetic fields. For the two-site spin system, we solve exactly the energy spectrum and phase diagram, also calculate the ground-state and thermal entanglements by using the concept of the concurrence. It is found that the two-site concurrence in the eigenstate which only depends on the imaginary magnetic field  $\eta$  is always equal to one in the region of  $\mathcal{PT}$  symmetry, while it decreases with  $\eta$  in the  $\mathcal{PT}$ -symmetric broken region. Especially, the concurrence shows the non-analytic behavior at the exceptional point, and the same is true in the case of the biorthogonal basis, which indicates that the concurrence can characterize the phase transition in this non-Hermitian system. The interesting thing is that  $\eta$  weakens the thermal entanglement when the system is isotropic and enhances the entanglement when the system becomes the Ising model. For the one-dimensional spin chain, the magnetization and entanglement are further studied by using the two-spin cluster mean-field approximation. The results show that their variations have opposite trends with the magnetic fields. Moreover, the system exists the first-order quantum phase transitions for some anisotropic parameters in the  $\mathcal{PT}$ -symmetry region, and the entanglement changes suddenly at the quantum phase transition point.

Keywords: Entanglement; Concurrence; Non-Hermitian XY system;  $\mathcal{PT}$  symmetry; Exceptional point; Mean-field theory

---

\*Corresponding author. E-mail address: kongxm668@163.com (X.-M. Kong).

## I. INTRODUCTION

As we have learned, Hamiltonians are required to be Hermitian in quantum mechanics, to ensure that the eigenvalues of Hamiltonians are real and the unitarity of evolution of the system state over time. Hermitian Hamiltonians generally describe closed systems, while the quantum systems which interact with the external environment can be represented by equivalent non-Hermitian Hamiltonians [1]. To explore these kinds of questions, as early as 1943, W. Pauli proposed the non-Hermitian operator and its theory of self-consistent inner product, which created a precedent in the study of non-Hermitian quantum theories [2, 3], and there are plenty of studies on non-Hermitian systems subsequently [4–9]. In 1998, Bender and Boettcher studied the systems with non-Hermitian Hamiltonians more deeply and found that non-Hermitian Hamiltonians with parity and time-reversal ( $\mathcal{PT}$ ) symmetry can still have full real spectrums [10]. And it made a tremendous contribution to research and development of non-Hermitian quantum mechanics.

In recent years, many studies have been done on non-Hermitian systems in theory and experiment and have found interesting phenomena that do not exist in Hermitian systems. Theoretically, there have been a large number of researches on the non-Hermitian in skin effect, generalized topological phases, the new non-Hermitian universalities, and so on [11–17]. Experimentally, a lot of work has been studied in quantum information, quantum optical systems, photonic crystals, mechanical systems, biological systems, and other fields [18–24].

It is well known that quantum entanglement plays an important role in various fields such as quantum information, condensed matter physics and statistical physics [25–27] and it is a characteristic of quantum systems, which provides a unique method for exploring the properties of quantum many-body systems. In particular, it has become a significant concept in condensed matter physics for characterizing and exploring the phases of matter [28, 29]. For the past few years, a number of inspiring advances have been made in the study of quantum entanglement and quantum phase transition [30–33]. In the fields of black hole physics, holography and non-equilibrium quantum dynamics, different entanglement measures have also attracted widespread attention [34–37]. There is also much work that has been done on the entanglement properties of the Hermitian spin systems [38–43]. The measurement of entanglement has also been achieved in experiments, such as the entanglement entropy

[44, 45].

Some meaningful and pioneering work has been done on the entanglement characteristics of non-Hermitian fermion systems, such as non-Hermitian topology and quantum quenching in non-Hermitian Hamiltonians [46–49]. However, there are few studies on the entanglement properties in non-Hermitian spin systems [50, 51]. In particular, there are very few studies using concurrence to measure it. For the spin systems, the XY systems are widely investigated, for instance, quantum entanglement, quantum discord, dynamics of quantum coherence, quantum Fisher information, and other aspects [52–55]. The interest about XY systems is due to experimental work on quasicrystals and quasiperiodic superlattices [56]. We study the ground-state and thermal entanglements respectively in the non-Hermitian spin-1/2 XY system by using concurrence as an entanglement measurement method and the mean-field theory in this manuscript. The purpose is to find the influence of the non-Hermitian term on entanglement and some peculiar properties of the system.

The organizational structure of this manuscript is as follows: In Sec. II, we introduce the non-Hermitian XY model and discuss the  $\mathcal{PT}$  symmetry of the system. The ground-state phase diagram is studied in Sec. III. In Sec. IV and V, the ground-state entanglement is discussed. Sec. VI studies the thermal entanglement. The magnetization and thermal entanglement are investigated by mean-field approximation in Sec. VII. We summarize our results in Sec. VIII.

## II. MODEL AND EXCEPTIONAL POINT

The Hamiltonian of the non-Hermitian spin-1/2 XY system in a one-dimensional lattice is

$$H = -\frac{J}{2} \sum_{l=1}^N [(1 + \gamma) \sigma_l^x \sigma_{l+1}^x + (1 - \gamma) \sigma_l^y \sigma_{l+1}^y] - h \sum_{l=1}^N \sigma_l^z + i\eta \sum_{l=1}^N (-1)^l \sigma_l^z, \quad (1)$$

where  $\sigma_l^\alpha$  ( $\alpha = x, y, z$ ) are the Pauli operators and satisfy the periodic boundary condition  $\sigma_l^\alpha = \sigma_{l+N}^\alpha$ ,  $N$  is the number of sites (spins) in the system.  $J$  is the nearest neighbor exchange coupling constant ( $J > 0$  and  $J < 0$  represent ferromagnetic and anti-ferromagnetic systems, respectively),  $\gamma$  is the anisotropic parameter,  $h$  is the external magnetic field and  $i\eta$  an imaginary, transverse magnetic field.  $\eta$  is a real number which measures the deviation of  $H$  from Hermiticity. If  $\eta$  is large enough to make complex some of the eigenvalues of  $H$ , this symmetry is spontaneously broken [57].

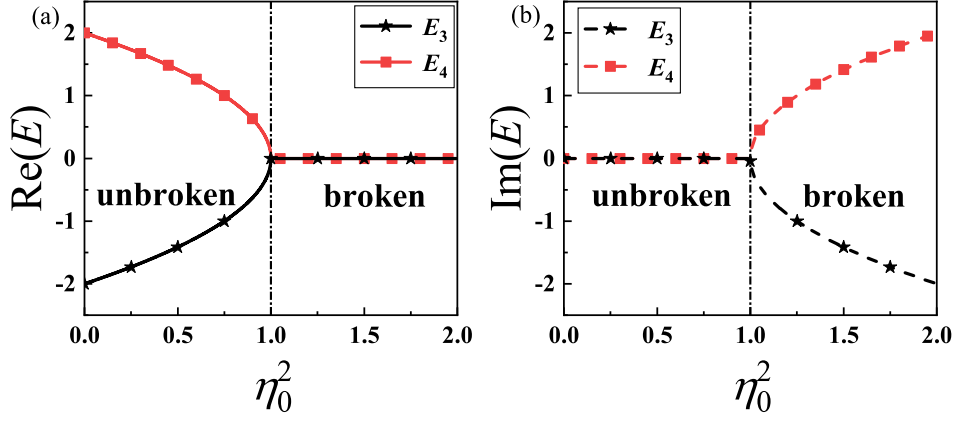


FIG. 1. The real and imaginary parts of the eigenvalues  $E_3$  and  $E_4$  as the functions of the square of the imaginary magnetic field. (a) the real parts of  $E_3$  and  $E_4$ , (b) the imaginary parts of  $E_3$  and  $E_4$ .  $\eta_0^2 < 1$  is the  $\mathcal{PT}$ -symmetric region and  $\eta_0^2 > 1$  is the  $\mathcal{PT}$ -symmetric broken one. The exceptional point occurs at  $\eta_0^2=1$ .

In this section, we study the XY model with two sites when  $J > 0$  whose Hamiltonian is

$$H = -\frac{J}{2} [(1 + \gamma) (\sigma_1^x \sigma_2^x + \sigma_2^x \sigma_1^x) + (1 - \gamma) (\sigma_1^y \sigma_2^y + \sigma_2^y \sigma_1^y)] - h(\sigma_1^z + \sigma_2^z) + i\eta(-\sigma_1^z + \sigma_2^z). \quad (2)$$

The eigenvalues and corresponding eigenstates of the Hamiltonian (2) are written as

$$E_1 = -2J\sqrt{h_0^2 + \gamma^2}, \quad |\varphi_1\rangle = \frac{1}{\sqrt{\gamma^2 + d_1^2}} [d_1 |\uparrow\uparrow\rangle + \gamma |\downarrow\downarrow\rangle], \quad (3a)$$

$$E_2 = 2J\sqrt{h_0^2 + \gamma^2}, \quad |\varphi_2\rangle = \frac{1}{\sqrt{\gamma^2 + d_2^2}} [d_2 |\uparrow\uparrow\rangle + \gamma |\downarrow\downarrow\rangle], \quad (3b)$$

$$E_3 = -2J\sqrt{1 - \eta_0^2}, \quad |\varphi_3\rangle = \frac{1}{\sqrt{1 + |d_3|^2}} [d_3 |\uparrow\downarrow\rangle + |\downarrow\uparrow\rangle], \quad (3c)$$

$$E_4 = 2J\sqrt{1 - \eta_0^2}, \quad |\varphi_4\rangle = \frac{1}{\sqrt{1 + |d_4|^2}} [d_4 |\uparrow\downarrow\rangle + |\downarrow\uparrow\rangle], \quad (3d)$$

where  $h_0 = h/J$  and  $\eta_0 = \eta/J$  are the reduced real magnetic field and imaginary magnetic field, respectively, as well as

$$\begin{aligned} d_1 &= h_0 + \sqrt{h_0^2 + \gamma^2}, \quad d_2 = h_0 - \sqrt{h_0^2 + \gamma^2}, \\ d_3 &= i\eta_0 + \sqrt{1 - \eta_0^2}, \quad d_4 = i\eta_0 - \sqrt{1 - \eta_0^2}. \end{aligned} \quad (4)$$

On the basis of the above statement, it is seen that all the eigenvalues of  $H$  are real if and only if  $1 - \eta_0^2 \geq 0$ . Fig. 1 gives the variations of the real and imaginary parts of  $E_3$

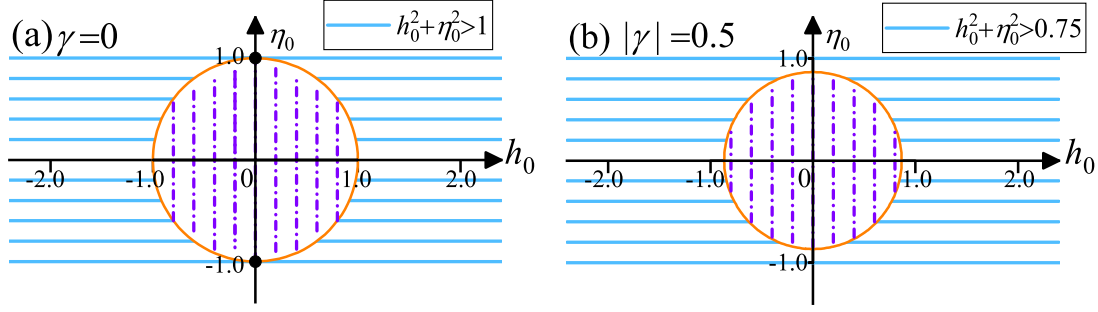


FIG. 2. Ground-state phase diagrams of the XY model with two sites. The shaded areas which are composed of transverse (blue) lines and vertical (purple) lines correspond to  $|\varphi_1\rangle$  and  $|\varphi_3\rangle$ , respectively.

and  $E_4$  with  $\eta_0^2$ , respectively. When  $\eta_0^2 < 1$ , the eigenvalues  $E_3$  and  $E_4$  remain real and the system is the  $\mathcal{PT}$ -symmetric. When  $\eta_0^2 > 1$ , the both eigenvalues are purely imaginary. At the moment, the system is in the  $\mathcal{PT}$ -symmetric broken region. The circle dot (blue) is the exceptional point (EP) at which the real and the imaginary parts of the eigenvalues are both zero and  $E_3 = E_4$  when  $\eta_0^2 = 1$ . Moreover, it also corresponds to the phase transition point from the  $\mathcal{PT}$ -symmetric phase to the broken one.

### III. GROUND-STATE PHASE DIAGRAM

On account of the previous discussion, we find that the ground state must be  $|\varphi_1\rangle$  or  $|\varphi_3\rangle$ . In this section, we discuss the conditions in which  $|\varphi_1\rangle$  and  $|\varphi_3\rangle$  are the ground states respectively or degenerate ground states. Fig. 2 is the ground-state phase diagram of the system and shows graphically the two possible ground states when  $\gamma = 0, 0.5$ .

The ground-state phase diagram in the  $h_0$ - $\eta_0$  plane is shown when  $\gamma = 0$  in Fig. 2(a) where the shaded area consisting of transverse (blue) lines (excluding (0,1) and (0,-1)), that is  $h_0^2 + \eta_0^2 > 1$ , corresponds to the ground state is  $|\varphi_1\rangle$ . While  $h_0^2 + \eta_0^2 < 1$ , then  $|\varphi_3\rangle$  is the ground state corresponding to the shaded area composing of vertical (purple) lines inside the circle. It corresponds to the circle (orange) border (Not including black circle dots) that  $|\varphi_1\rangle$  and  $|\varphi_3\rangle$  are degenerate ground states when  $h_0^2 + \eta_0^2 = 1$ .

In the case of  $0 < |\gamma| < 1$ ,  $|\varphi_3\rangle$  is the ground state, which is still possible. Without

loss of generality, Fig. 2(b) shows the ground-state phase diagram in the  $h_0$ - $\eta_0$  plane when  $|\gamma| = 0.5$ . In the case of  $h_0^2 + \eta_0^2 > 0.75$ ,  $|\varphi_1\rangle$  is the ground state which corresponds to the shaded area consisting of blue (transverse) lines. The shaded area consisting of purple (vertical) lines inside the circle is the case of  $h_0^2 + \eta_0^2 < 0.75$ , which corresponds to the ground state is  $|\varphi_3\rangle$ . When  $h_0^2 + \eta_0^2 = 0.75$ , both  $|\varphi_1\rangle$  and  $|\varphi_3\rangle$  are ground states, which corresponds to the orange (circle) border in Fig. 2(b).

When  $|\gamma| = 1$ , If real and imaginary magnetic fields are not zero simultaneously, then  $|\varphi_1\rangle$  is the ground state. Otherwise  $E_1 = E_3$ , the ground states are degenerate. When  $\gamma > 1$ ,  $h_0^2 + \eta_0^2 > 1 - \gamma^2$ ,  $|\varphi_1\rangle$  is the ground state certainly.

#### IV. GROUND-STATE ENTANGLEMENT

The previous section has discussed the ground state phase diagram of the system. The ground-state entanglement of the system is studied by using concurrence in this section. The concurrence is defined as [58]

$$C = \max \left[ 0, \sqrt{\lambda_1} - \sqrt{\lambda_2} - \sqrt{\lambda_3} - \sqrt{\lambda_4} \right], \quad (5)$$

where  $\lambda_j$  ( $j = 1, 2, 3, 4$ ) are the eigenvalues, in decreasing order, of the non-Hermitian matrix  $R = \rho \tilde{\rho}$ . Note that each  $\lambda_j$  is a non-negative real number [58].  $\rho$  is the density matrix, and  $\tilde{\rho}$  is the spin-flipped density matrix which can be written as  $\tilde{\rho} = (\sigma^y \otimes \sigma^y) \rho^* (\sigma^y \otimes \sigma^y)$ , where  $\rho^*$  is the complex conjugate of  $\rho$ .

##### (1) The case of $h_0^2 + \eta_0^2 > 1 - \gamma^2$

In this situation,  $|\varphi_1\rangle$  is the ground state which only depends on  $h_0$  and  $\gamma$ . The ground-state density matrix of the system is obtained as

$$\rho_{01} = \begin{pmatrix} a_1 & 0 & 0 & a_2 \\ 0 & 0 & 0 & 0 \\ 0 & 0 & 0 & 0 \\ a_3 & 0 & 0 & a_4 \end{pmatrix}, \quad (6)$$

where

$$a_1 = \frac{d_1^2}{\gamma^2 + d_1^2}, \quad a_2 = a_3 = \frac{\gamma d_1}{\gamma^2 + d_1^2}, \quad a_4 = \frac{\gamma^2}{\gamma^2 + d_1^2}. \quad (7)$$

Base on the definition, when the ground state is  $|\varphi_1\rangle$ , the concurrence can be written as

$$C_{01} = \frac{|\gamma|}{\sqrt{h_0^2 + \gamma^2}}. \quad (8)$$

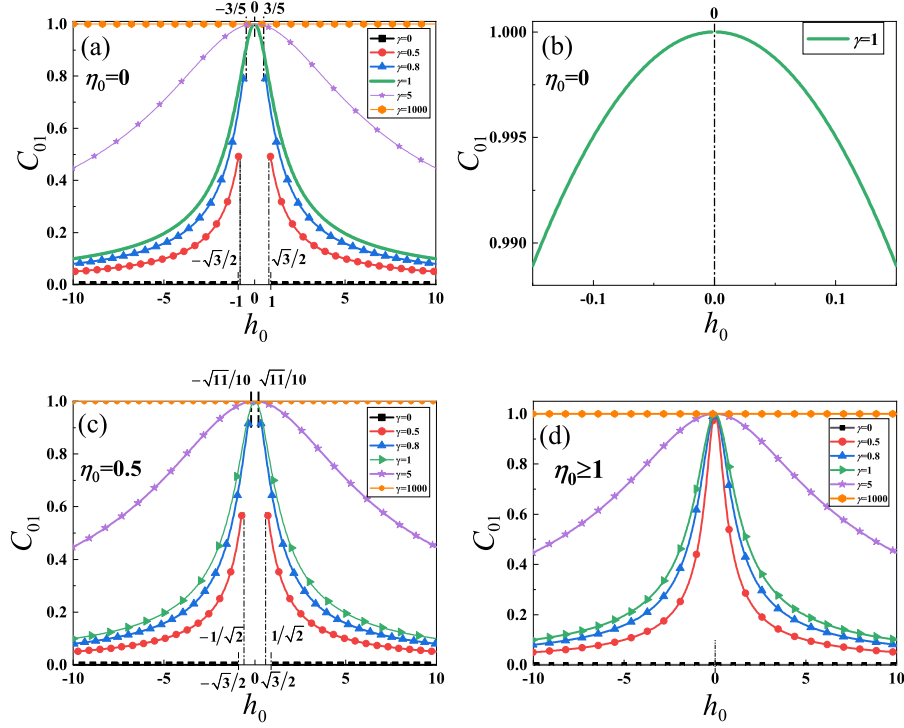


FIG. 3. Concurrence  $C_{01}$  versus the real magnetic field for different the anisotropy parameters and imaginary magnetic fields: (b) the entanglement behavior in the range of  $|h_0| < 0.15$  when  $\eta_0 = 0$ ,  $\gamma = 1$ . The range of  $h_0$  between the marked dashed line and the dashed line cannot take a value. Concurrence is zero (Square dot line) between two spins when  $\gamma = 0$ .

It can be seen that there is no entanglement between two spins when  $\gamma = 0$  and  $h_0 \neq 0$  within the value ranges of parameters discussed in the previous section. In this situation,  $|\varphi_1\rangle = |\uparrow\uparrow\rangle$  is a direct product state, which is consistent with the above case.

In the case of  $0 < |\gamma| < \infty$ , if  $h_0 = 0$ , then  $C_{01} = 1$  and  $|\varphi_1\rangle = \frac{1}{\sqrt{2}}[|\uparrow\uparrow\rangle + |\downarrow\downarrow\rangle]$ , the system is in the Bell state; the entanglement disappears, which occurs in  $|h_0| \rightarrow \infty$ . In addition, the entanglement between two spins also is the largest, which takes place when  $|\gamma| \rightarrow \infty$  and  $0 \leq |h_0| < \infty$ .

The above results can be seen more obviously in Fig. 3 which is the variations of concurrence with  $h_0$  for different  $\gamma$ . We also find that the anisotropic parameter enhances entanglement, while the real magnetic field weakens entanglement, and  $\eta_0$  only affects the value range of  $h_0$ . In the  $\mathcal{PT}$ -symmetric broken region, the ground state is  $|\varphi_1\rangle$  due to the

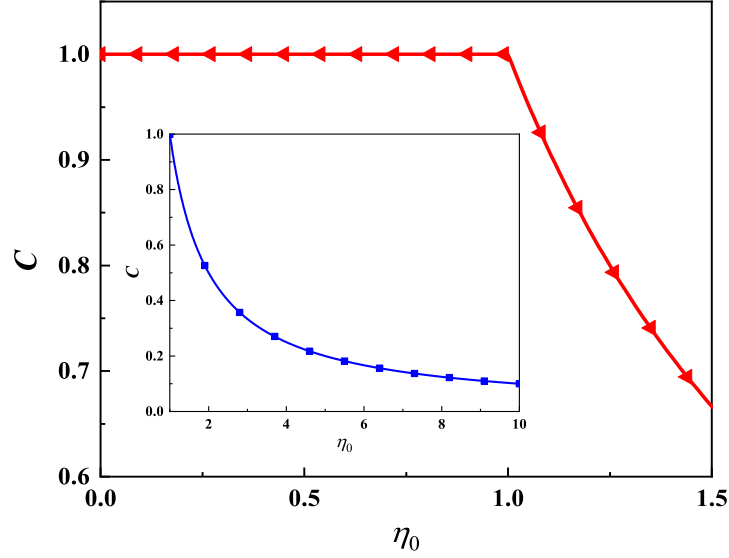


FIG. 4. Concurrence versus the imaginary magnetic field. The illustration shows concurrence when the system is in the  $\mathcal{PT}$ -symmetry broken region.

real part of  $E_3$  is zero and  $E_1$  is always less than zero when  $h_0$  and  $\gamma$  are not simultaneously zero [59]. Specially, the ground-state concurrence has the maximum when  $h_0 = 0$  at the exceptional point.

**(2) The case of  $h_0^2 + \eta_0^2 < 1 - \gamma^2$**

In this case,  $|\varphi_3\rangle$  which only depends on  $\eta_0$ , is the ground state. The ground-state density matrix of the system is

$$\rho_{02} = \begin{pmatrix} 0 & 0 & 0 & 0 \\ 0 & b_1 & b_2 & 0 \\ 0 & b_3 & b_4 & 0 \\ 0 & 0 & 0 & 0 \end{pmatrix}, \quad (9)$$

where

$$b_1 = b_4 = \frac{1}{1 + |d_3|^2}, \quad b_2 = \frac{d_3^*}{1 + |d_3|^2}, \quad b_3 = \frac{d_3}{1 + |d_3|^2}, \quad (10)$$

in which  $d_3^*$  is the complex conjugate of  $d_3$ .

In terms of Eq. (5), the ground-state concurrence is obtained as  $C_{02} = 1$ . In this case, the concurrence is always the maximum within the acceptable ranges of parameters and the system is in the Bell state. What's interesting is that concurrence is independent of the anisotropic parameter, real and imaginary magnetic fields.



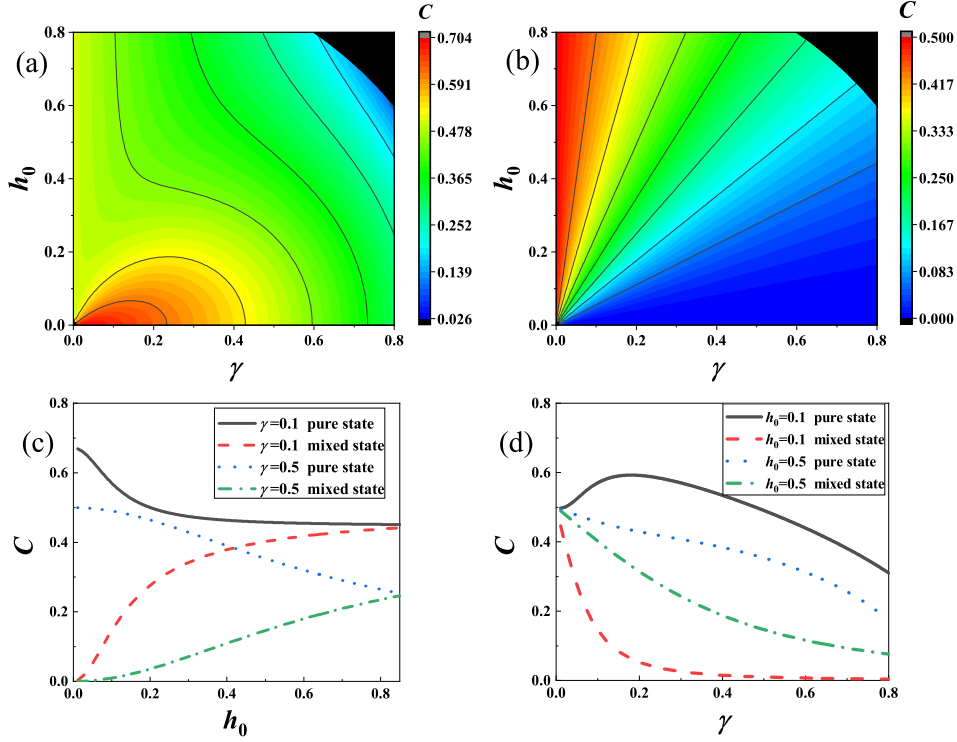


FIG. 5. The mixed-state and the pure-state entanglements of two ground-states. When  $\eta_0 = \sqrt{1 - h_0^2 - \gamma^2}$ , the variations of concurrence with  $h_0$  and  $\gamma$ : (a) The contour plot of pure-state entanglement. (b) The contour plot of mixed-state entanglement. The black area is a area where  $\gamma$  and  $h_0$  cannot take a value. (c) and (d) The entanglements of the mixed state and the pure state as functions of  $h_0$  when  $\gamma = 0.1$  and  $\gamma = 0.5$  and as functions of  $\gamma$  when  $h_0 = 0.1$  and  $h_0 = 0.5$ .

In order to study the properties of entanglement in the  $\mathcal{PT}$ -symmetric broken region [50], Fig. 4 shows that the concurrence of  $|\varphi_3\rangle$  varies with  $\eta_0$ . In the  $\mathcal{PT}$ -symmetric region, the concurrence is a constant, while it decreases with the increase of the imaginary magnetic field and tends to zero infinitely in the  $\mathcal{PT}$ -symmetric broken region ( $\eta_0 > 1$ ). Moreover, the concurrence shows the non-analytic behavior at the exceptional point.

### (3) The case of $h_0^2 + \eta_0^2 = 1 - \gamma^2$

On the basis of the Hamiltonian and the above results, it is found that the entanglement curves are axially symmetric concerning zero. Without loss of generality, the following discussions only focus on the case where each parameter is greater than zero. Next, we

study the ground-state entanglement when  $|\varphi_1\rangle$  and  $|\varphi_3\rangle$  are degenerate ground states.

When the superposition of ground states  $|\varphi_1\rangle$  and  $|\varphi_3\rangle$  is a pure state, that is,  $|\varphi_0\rangle = d_1 |\varphi_1\rangle + d_2 |\varphi_3\rangle$ , where  $d_1$  and  $d_2$  are constants, thus the density matrix is  $\rho = |\varphi_0\rangle \langle \varphi_0|$ . Moreover, we obtain the entanglement of the pure state when  $d_1 = d_2$ .

When the superposition of  $|\varphi_1\rangle$  and  $|\varphi_3\rangle$  is a mixed state, the density matrix is written as  $\rho = |\varphi_1\rangle p_1 \langle \varphi_1| + |\varphi_3\rangle p_2 \langle \varphi_3|$ . Assume that  $p_1 = p_2$ , the mixed-state entanglement is obtained.

We show the variation of pure-state entanglement with  $h_0$  and  $\gamma$  when  $\eta_0 = \sqrt{1 - h_0^2 - \gamma^2}$  ( $0 < h_0^2 + \gamma^2 \leq 1$ ) in Fig. 5(a) and find that the concurrence decreases with the increasing  $h_0$ , which is opposite of the entanglement of the mixed state in Fig. 5(b). Fig. 5(c) is the variations of the pure-state entanglement and the mixed-state one with  $h_0$  when  $\gamma = 0$  and  $\gamma = 0.5$ , and we find that the former is greater than the latter. Furthermore, the pure-state entanglement first increases and then decreases with the increasing  $\gamma$  when  $h_0 = 0.1$  in Fig. 5(d), which is also consistent with the change rule of Fig. 5(a).

## V. BI-ORTHOGONAL BASIS

Due to non-Hermitian Hamiltonian  $H \neq H^\dagger$ , the eigenvalue equations of  $H$  and  $H^\dagger$  are given by [60, 61]

$$H |\varphi_n\rangle = E_n |\varphi_n\rangle, \quad \langle \varphi_n| H^\dagger = \langle \varphi_n| E_n^* \quad (11)$$

$$H^\dagger |\phi_m\rangle = E'_m |\phi_m\rangle, \quad \langle \phi_m| H = \langle \phi_m| E'_m{}^* \quad (12)$$

where

$$\langle \phi_m| \varphi_n\rangle = \delta_{mn}. \quad (13)$$

On the basis, the biorthogonal density matrix can be written as

$$\rho = |\varphi_n\rangle \langle \phi_n|. \quad (14)$$

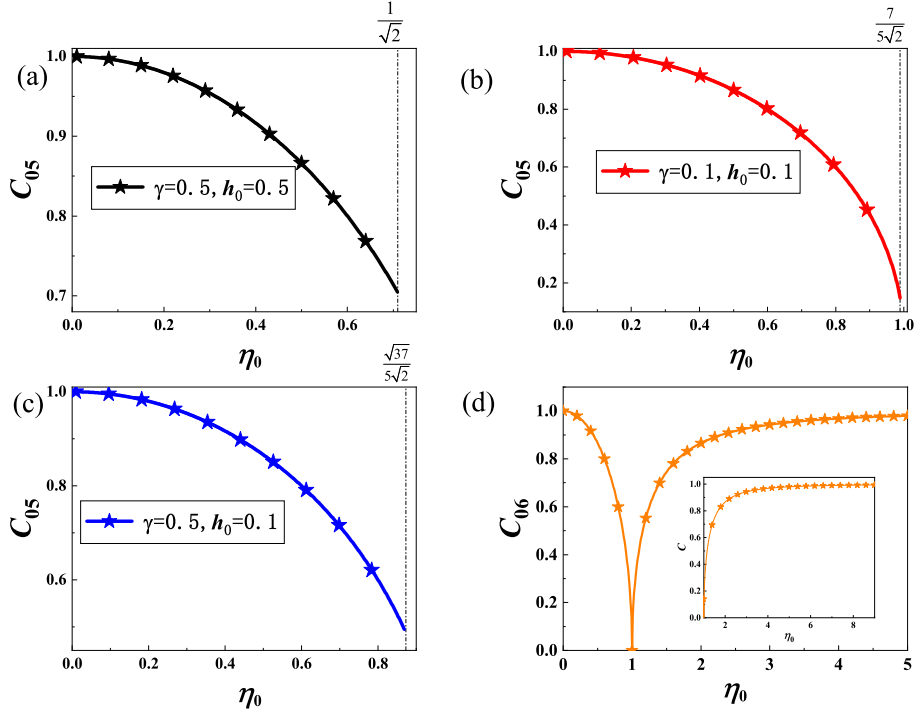


FIG. 6. Concurrence versus imaginary magnetic field. (a), (b) and (c) are the change of ground-state concurrence with  $\eta_0$  for different  $\gamma$  and  $h_0$  in the  $\mathcal{PT}$ -symmetry region. The range of  $\eta_0$  between zero and the marked dashed line can take values. (d) The concurrence of  $|\varphi_3\rangle$ . The illustration shows concurrence when the system is in the  $\mathcal{PT}$ -symmetry broken region.

The eigenvalues and corresponding eigenstates of  $H^\dagger$  are obtained as

$$E'_1 = -2J\sqrt{h_0^2 + \gamma^2}, \quad |\phi_1\rangle = \frac{1}{\sqrt{\gamma^2 + d_1^2}} [d_1 |\uparrow\uparrow\rangle + \gamma |\downarrow\downarrow\rangle], \quad (15a)$$

$$E'_2 = 2J\sqrt{h_0^2 + \gamma^2}, \quad |\phi_2\rangle = \frac{1}{\sqrt{\gamma^2 + d_2^2}} [d_2 |\uparrow\uparrow\rangle + \gamma |\downarrow\downarrow\rangle], \quad (15b)$$

$$E'_3 = -2J\sqrt{1 - \eta_0^2}, \quad |\phi_3\rangle = \frac{1}{\sqrt{1 + |d_3^*|^2}} [d_3^* |\uparrow\downarrow\rangle + |\downarrow\uparrow\rangle], \quad (15c)$$

$$E'_4 = 2J\sqrt{1 - \eta_0^2}, \quad |\phi_4\rangle = \frac{1}{\sqrt{1 + |d_4^*|^2}} [d_4^* |\uparrow\downarrow\rangle + |\downarrow\uparrow\rangle]. \quad (15d)$$

When  $|\varphi_3\rangle$  is the ground state, the biorthogonal density matrix is

$$\rho_{03} = \begin{pmatrix} 0 & 0 & 0 & 0 \\ 0 & x_1 & x_2 & 0 \\ 0 & x_3 & x_4 & 0 \\ 0 & 0 & 0 & 0 \end{pmatrix}, \quad (16)$$

where

$$\begin{aligned} x_1 &= \frac{d_3^2}{\sqrt{(1+|d_3|)(1+|d_3^*|)}}, \quad x_2 = \frac{d_3}{\sqrt{(1+|d_3|)(1+|d_3^*|)}}, \\ x_3 &= \frac{d_3}{\sqrt{(1+|d_3|)(1+|d_3^*|)}}, \quad x_4 = \frac{1}{\sqrt{(1+|d_3|)(1+|d_3^*|)}}. \end{aligned} \quad (17)$$

According to the definition Eq. (5), the ground-state concurrence of the system can be obtained in the case of biorthogonal basis in Figs. 6(a)–(c), and it decreases with increasing  $\eta_0$ . In this case, the entanglement of this non-Hermitian system is smaller than that of the Hermitian system ( $\eta_0 = 0$ ), which is different from the case of the density matrix of  $|\varphi_3\rangle$  in the region of PT symmetry. When  $|\varphi_1\rangle$  is the ground state, the concurrence is identical with the case of  $\rho_{01}$  due to  $|\varphi_1\rangle = |\phi_1\rangle$ .

The variations of concurrence in biorthogonal basis of  $|\varphi_3\rangle$  are shown in Fig. 6(d). It is found that the trends of entanglement in the  $\mathcal{PT}$ -symmetry region and broken region are inverse. At the exceptional point, the entanglement is reduced to the minimum, which is the opposite of the result in Fig. 4, and has the non-analytic behavior.

## VI. THERMAL ENTANGLEMENT

In this section, the thermal entanglement of the system is studied in the  $\mathcal{PT}$ -symmetry region. The density matrix is defined as  $\rho = \exp(-\beta H)/Z$ , in which  $\beta = 1/k_B T$ ,  $k_B$  is the Boltzmann constant,  $T$  is temperature, and  $Z = \text{Tr}[\exp(-\beta H)]$  is the partition function in the canonical ensemble. In this way, we obtain the density matrix and concurrence of the system.

Fig. 7 shows the variations of the concurrence with temperature for different  $\eta_0$  and  $\gamma$ . We find that the concurrence decreases with the increase of  $\eta_0$  at the same temperature when  $\gamma = 0$ , and the larger  $\eta_0$  is, the faster the concurrence decreases. When  $\gamma = 0.5$ , the concurrence first decreases then increases with the increase of  $\eta_0$ , which can be seen more

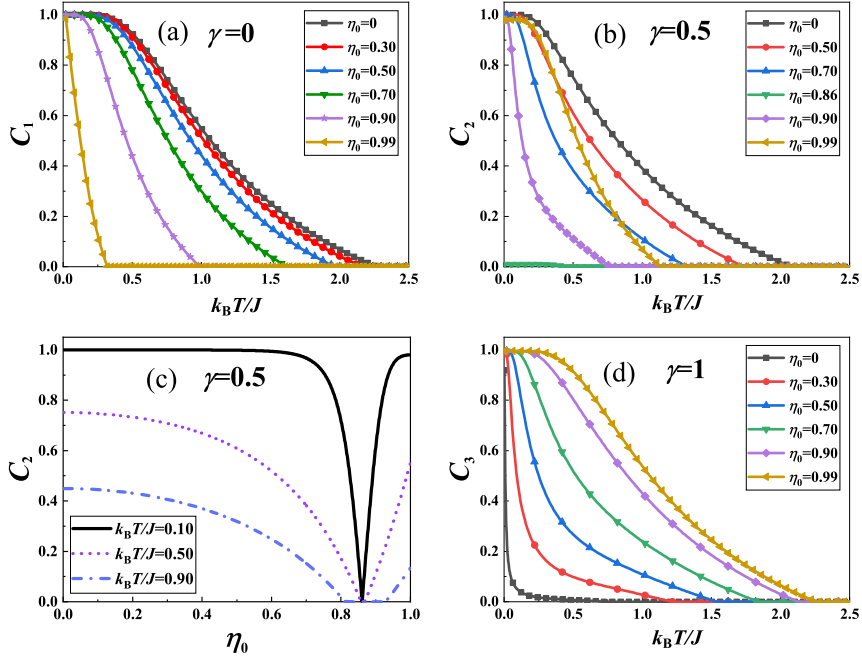


FIG. 7. The thermal entanglements between two spins for different values of the anisotropy parameters and imaginary magnetic fields when  $h_0 = 0.1$ : (a)  $\gamma = 0$ , entanglement is the maximum when  $\eta_0 = 0$ . (b)  $\gamma = 0.5$ , the thermal entanglement as a function of temperature. (c)  $\gamma = 0.5$ , the thermal entanglement as functions of  $\eta_0$  for different values of temperature. (d)  $\gamma = 1$ , entanglement is the minimum when  $\eta_0 = 0$ .

intuitively in Fig. 7(c), and it reduces to a minimum when  $\eta_0 = 0.86$  due to the ground state is degenerate in this point. For  $\gamma = 1$ , the concurrence increases with the increase of  $\eta_0$ , and it indicates that the entanglement of this non-Hermitian system is greater than that of the Hermitian system ( $\eta_0 = 0$ ), which is opposite of the case when  $\gamma = 0$ .

Fig. 8(a) shows the variations of the concurrence with temperature for different  $h_0$  and  $\eta_0$  when  $\gamma = 0$ . Due to the energy level crossing, the concurrence can change suddenly when the magnetic field near 0.99 as  $k_B T/J \rightarrow 0$ . In addition, it decreases with the increase of  $h_0$  at the same temperature when  $\eta_0 = 0.1$  and reduces directly to zero with the increase of temperature when  $0 \leq h_0 \leq 0.99$ . It is worth noticing that the concurrence first increases and then decreases with the increasing temperature when  $h_0 > 0.99$ . We can obviously see that the concurrence under different external magnetic fields becomes zero at the same temperature in the illustration, which indicates that the threshold temperature is indepen-

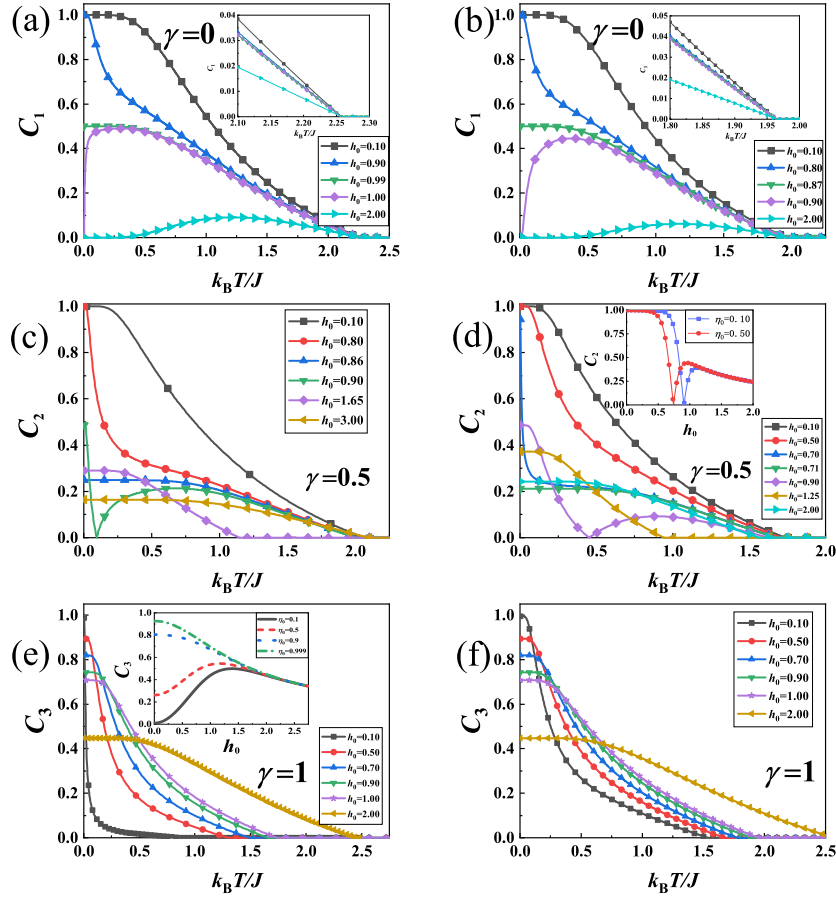


FIG. 8. The thermal entanglements between two spins as the functions of temperature for different values of real and imaginary magnetic fields when  $\gamma = 0, 0.5$  and  $1$ . (a), (c) and (e) are  $\eta_0 = 0.1$  and (b), (d) and (f) are  $\eta_0 = 0.5$ . (a) the illustration shows the behavior of concurrence at a temperature around  $2.1$  to  $2.3$ . (b) the illustration shows the behavior of concurrence at a temperature around  $1.8$  to  $2.0$ . (d) the illustration shows variation of concurrence with  $h_0$  when  $\gamma = 0.5$ ,  $k_B T/J = 0.1$ . (e) the illustration shows variation of concurrence with  $h_0$  when  $\gamma = 1$ ,  $k_B T/J = 0.5$ .

dent of  $h_0$ . When  $\eta_0 = 0.5$ , the variations of concurrence with temperature are shown in Fig. 8(b), which is similar to the case when  $\eta_0 = 0.1$ , and the point of sudden change is in  $h_0 = 0.87$ . The concurrence decreases faster with the increase of temperature, and the temperature at which eventually becomes zero is smaller than that in Fig. 8(a), which is consistent with the result when  $\gamma = 0$  in Fig. 7. Furthermore, we find that the larger  $\eta_0$  is,

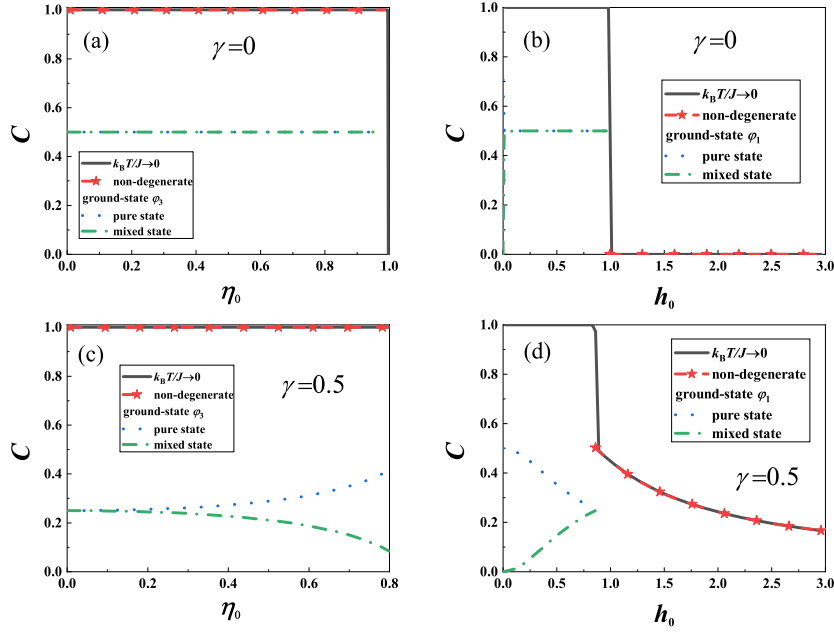


FIG. 9. The comparison between thermal entanglement as  $k_B T/J \rightarrow 0$ , the pure-state, mixed-state and non-degenerate ground-state entanglements. (a) and (c): Black (Solid) and red (star) lines correspond to  $h_0 = 0.1$ . Blue (dotted) and green (chain) lines correspond to  $h_0 = \sqrt{1 - \eta_0^2 - \gamma^2}$ . (b) and (d): Black (Solid) and red (star) lines correspond to  $\eta_0 = 0.1$ . Dotted (blue) and chain (green) lines correspond to  $\eta_0 = \sqrt{1 - h_0^2 - \gamma^2}$ .

the smaller  $h_0$  corresponding to the point of sudden change of concurrence.

In Fig. 8(c), the variations of the concurrence with temperature are shown for different  $h_0$  and  $\eta_0$  when  $\gamma = 0.5$ . For  $\eta_0 = 0.1$ , we find that the concurrence reduces directly to zero with the increasing temperature when  $0 \leq h_0 \leq 0.86$ . When  $h_0 > 0.86$ , the concurrence first decreases, then increases, and then decreases to zero with the increase of temperature. When  $h_0$  increases to around 1.65, the concurrence decreases directly to zero with the increase of temperature. The concurrence first decreases, then increases, and then decreases with the increase of  $h_0$  when  $k_B T/J \rightarrow 0$ , and this is more evident in the inset of Fig. 8(d). For  $\eta_0 = 0.5$ , the concurrence is similar to the case when  $\eta_0 = 0.1$ . The point of sudden change is obtained in  $h_0 = 0.71$ . The temperature at which the concurrence eventually becomes zero is smaller, and it is consistent with the result when  $\gamma = 0.5$  in Fig. 7.

Fig. 8(e) and Fig. 8(f) show the variations of concurrence with temperature for different  $h_0$  and  $\eta_0$  when  $\gamma = 1$ , respectively. It is observed that the concurrence decreases with the increase of  $h_0$  when  $k_B T/J \rightarrow 0$ , while the real magnetic field enhances entanglement when the temperature becomes higher. It is also found that the smaller  $h_0$  is, the faster the concurrence decreases. When  $h_0 = 2$ , the variation of concurrence with temperature for  $\eta_0 = 0.1$  is identical to that of  $\eta_0 = 0.5$ , as a consequence the concurrence is independent of  $\eta_0$  in this case, which can be seen more distinctly from the illustration in Fig. 8(e). The concurrence decreases smoothly to zero with the increasing temperature when  $\gamma = 1$ , which is different from  $\gamma = 0$  and  $\gamma = 0.5$ , due to the system becomes Ising model at this moment.

In order to compare the thermal entanglement as  $k_B T/J \rightarrow 0$ , the pure-state, mixed-state and non-degenerate ground-state entanglements, Fig. 9 shows their variations with  $h_0$  and  $\eta_0$ . It can be seen that, within the ranges of available values, the pure-state and mixed-state entanglements are overlapped partially. When  $k_B T/J \rightarrow 0$ , the thermal and the non-degenerate ground-state entanglements have overlapping parts. It is indicated that the thermal entanglement is realized by non-degenerate ground states in this case.

## VII. RESULT OF MEAN-FIELD THEORY

Based on the previous discussions of two-site spin system, we study the magnetization and entanglement of the non-Hermitian spin-1/2 XY spin chain by using the mean-field theory in this section. According to the two-spin cluster mean-field approximation [62, 63], the many-body system is transformed into the two-body system, and the two-spin cluster Hamiltonian can be written as

$$H_{MFA} = -\frac{J}{2} [(1 + \gamma) (\sigma_1^x \sigma_2^x + \sigma_2^x \sigma_1^x) + (1 - \gamma) (\sigma_1^y \sigma_2^y + \sigma_2^y \sigma_1^y)] \quad (18)$$

$$- h(\sigma_1^z + \sigma_2^z) + i\eta(-\sigma_1^z + \sigma_2^z) - Jm(q - 1)(\sigma_1^z + \sigma_2^z),$$

where  $m = \langle \frac{1}{2} (\sigma_1^z + \sigma_2^z) \rangle$  is the magnetization along the fixed direction  $z$  in space. In terms of above method, the average effective Hamiltonian of two-spin cluster is

$$\tilde{H}_{MFA} = -\frac{J}{2} [(1 + \gamma) (\sigma_1^x \sigma_2^x + \sigma_2^x \sigma_1^x) + (1 - \gamma) (\sigma_1^y \sigma_2^y + \sigma_2^y \sigma_1^y)] - h(\sigma_1^z + \sigma_2^z) \quad (19)$$

$$+ i\eta(-\sigma_1^z + \sigma_2^z) - Jm(q - 1)(\sigma_1^z + \sigma_2^z) + J(q - 1)m^2,$$



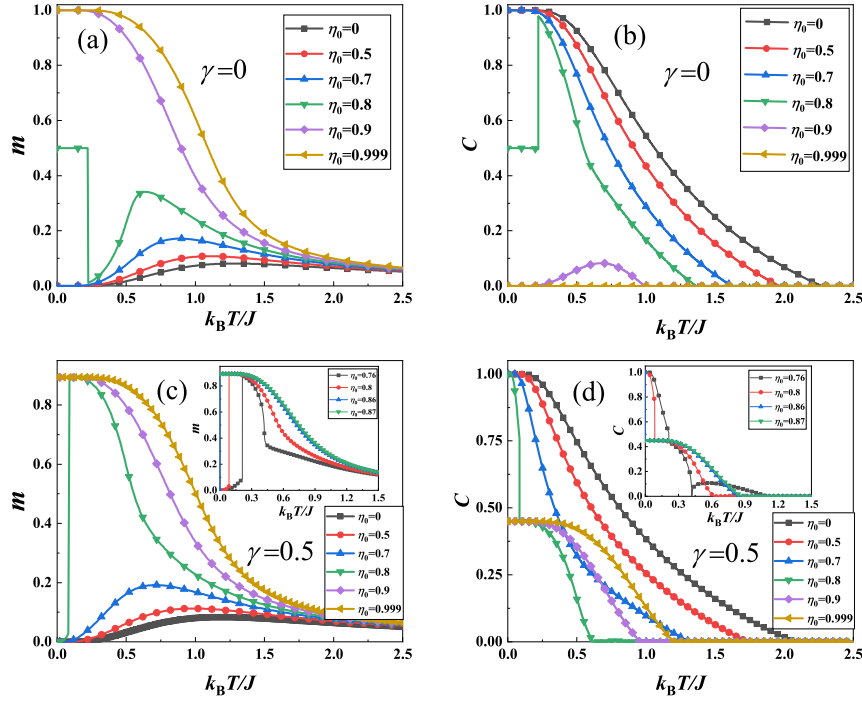


FIG. 10. The magnetization and concurrence as the functions of temperature for several different the imaginary magnetic fields when  $\gamma = 0, 0.5$  and  $h_0 = 0.1$ . They have the opposite change trends, that is, the magnetization increases when the concurrence decreases, and change suddenly when  $\eta_0 = 0.8$ . The insets of (c) and (d) show the variations of the magnetization and the concurrence with temperature around  $\eta_0 = 0.8$ .

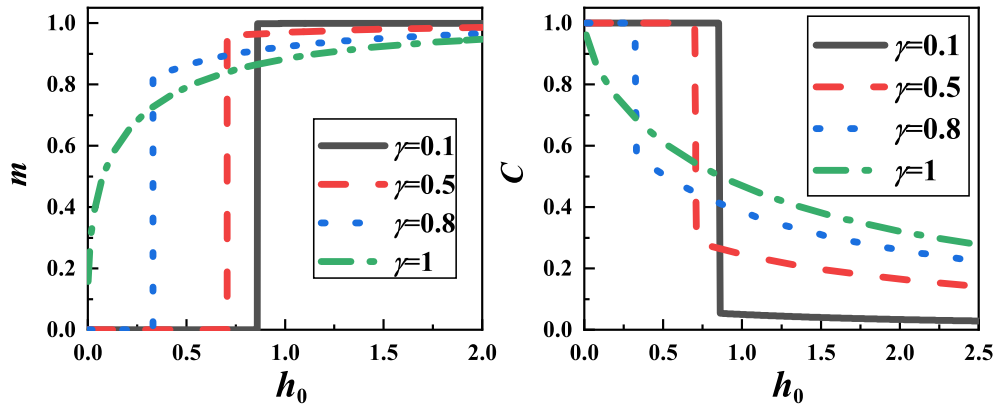


FIG. 11. The magnetization and concurrence as the functions of the magnetic field for several different the anisotropy parameters as  $k_B T/J \rightarrow 0$ . They have the opposite change trends, and their points of sudden change are the same.

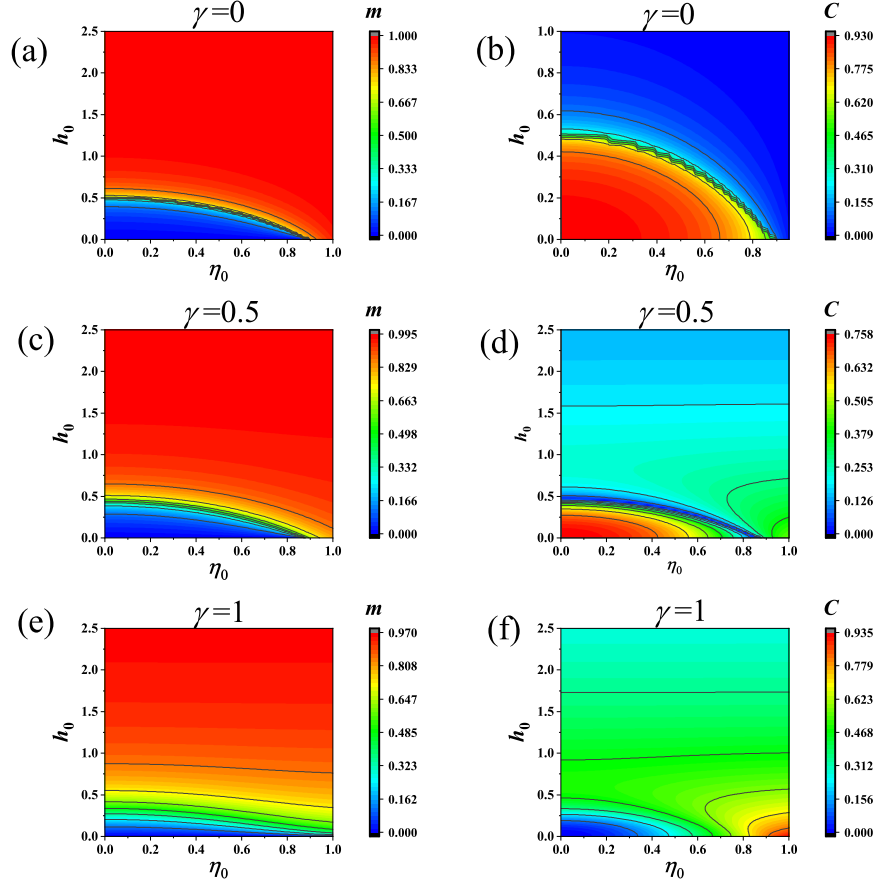


FIG. 12. The contour plots of the magnetization and the concurrence for three different the anisotropy parameters when  $k_B T/J = 0.5$ . (a), (c) and (e) are the contour plots of the magnetization. (b), (d) and (f) are the contour plots of the concurrence.

and the free energy as a function of the temperature  $T$  and magnetization  $m$  is given by

$$F = -k_B T \ln \tilde{Z} = J(q-1)m^2 - k_B T \ln Z, \quad (20)$$

where  $\tilde{Z} = \text{Tr}[\exp(-\beta \tilde{H}_{MFA})]$  and  $Z = \text{Tr}[\exp(-\beta H_{MFA})]$ . By the equilibrium condition  $\partial F / \partial m = 0$  of the system, the magnetization  $m$  is obtained as

$$m = \frac{[h_0 + m(q-1)] \sinh\left(\frac{2J\sqrt{[h_0 + m(q-1)]^2 + \gamma^2}}{k_B T}\right)}{\sqrt{[h_0 + m(q-1)]^2 + \gamma^2} \left[ \cosh\left(\frac{2J\sqrt{[h_0 + m(q-1)]^2 + \gamma^2}}{k_B T}\right) + \cosh\left(\frac{2J\sqrt{1-\eta^2}}{k_B T}\right) \right]}. \quad (21)$$

On the basis of the previous discussion, without loss of generality, we only calculate a few outstanding results. In Fig. 10, we obtain the variations of the magnetization and the

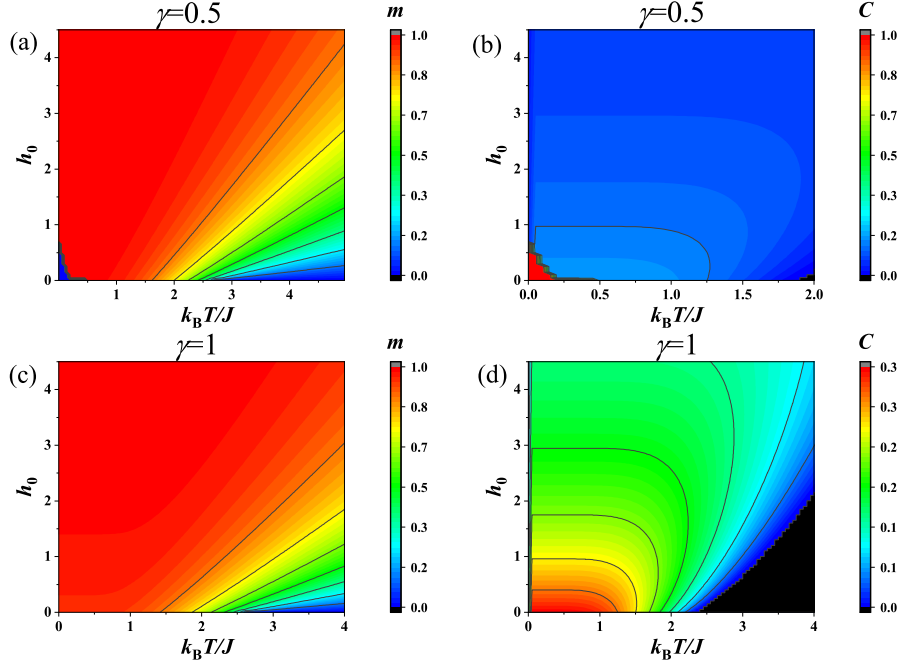


FIG. 13. The contour plots of the magnetization and the concurrence with the real magnetic field and temperature when  $q = 4$ . (a) and (c) are the contour plots of the magnetization. (b) and (d) are the contour plots of the concurrence.

concurrence with temperature for different  $\eta_0$  when  $\gamma = 0, 0.5$  and  $h_0 = 0.1$  and find that the magnetization increases and the concurrence decreases with the increase of  $\eta_0$  at the same temperature in Figs. 10(a) and (b), furthermore, their variations have opposite trends with temperature, which is caused by two-spin cluster mean-field approximation used in Eq. (19). When  $\eta_0 = 0.8$ , the magnetization and entanglement become 0.5 at  $k_B T/J = 0$  due to the ground states are degenerate, and their sudden change which is the result of the self-consistent equation Eq. (21), which is different from the result of the two-site system. In addition, the concurrence is maximum when  $\eta_0 = 0$ , which implies that the entanglement of this non-Hermitian system is smaller than one of the Hermitian system ( $\eta_0 = 0$ ). This is similar to the case of the system of two sites. From Figs. 10(c) and (d), the magnetization and the concurrence change suddenly as  $\eta_0$  increases to around 0.8, which can be seen more clearly in the illustrations, and the maximum value of entanglement becomes smaller when  $\eta_0 > 0.86$  and  $k_B T/J = 0$ . Furthermore, the temperature at which entanglement finally reduces to zero decreases and then increases with the increase of  $\eta_0$ .

In Fig. 11, the magnetization and the concurrence are presented as functions of  $h_0$  for

four different  $\gamma$  when  $\eta_0 = 0.5$  and  $k_B T/J \rightarrow 0$ , and their variations have opposite trends with the magnetic field. As we can see in the figure, the discontinuities in the magnetization and the entanglement occur when  $\gamma < 1$  in which the system undergoes first-order quantum phase transitions. Fig. 12 is the contour plots of the magnetization and the concurrence with  $h_0$  and  $\eta_0$  for three different  $\gamma$  when  $k_B T/J = 0.5$ . The magnetization increases with the increase of the magnetic field, and the concurrence is consistent with the previous analysis in Fig. 10 for the same case. Especially, the entanglement first decreases and then increases with  $\eta_0$  when  $\gamma = 0.5$  and  $h_0$  is small. In addition, the changes of the magnetization and the concurrence have the same trends when  $\gamma = 1$ , which is different from the case of  $k_B T/J \rightarrow 0$  in Fig. 11.

The properties of the one-dimensional systems have been introduced in the previous sections, and the high-dimensional systems also can be discussed by this mean-field method. In Fig. 13, the contour plots of the magnetization and the concurrence with  $h_0$  and  $k_B T/J$  for two different  $\gamma$  when  $\eta_0 = 0.5$  in the two-dimensional ( $q = 4$ ) system are shown. We find that it is similar to the one-dimensional case but the temperature at which the concurrence finally reaches zero is higher in the two-dimensional case than in the one-dimensional case and the entanglement of the three-dimensional system also is similar, whereas aforementioned the temperature is higher.

## VIII. CONCLUSIONS

In this manuscript, we have studied the ground-state and thermal entanglements of the non-Hermitian spin-1/2 XY model. In  $\mathcal{PT}$ -symmetric region, it is found that the two-site entanglement of  $|\varphi_3\rangle$  is independent of the imaginary magnetic field  $\eta_0$ , while  $\eta_0$  weakens the entanglement for the case of the biorthogonal basis in the two-site system. Moreover, the concurrence of  $|\varphi_3\rangle$  shows the non-analytic behavior at the exceptional point, and it indicates that the concurrence can characterize the phase transition in this non-Hermitian system. In addition, there are the first-order quantum phase transitions in this one-dimensional chain for some anisotropic parameters in the region of  $\mathcal{PT}$  symmetry, and the entanglement changes suddenly at the quantum phase transition point. For thermal entanglement, the imaginary magnetic field weakens it when the system is isotropic and enhances it when the anisotropy parameter  $\gamma = 1$  (Ising model).

## Acknowledgments

This work is supported by the National Natural Science Foundation of China under Grants No. 11675090, and No. 11905095; Shandong Provincial Natural Science Foundation, China under Grant No. ZR202111160185. Y. Li. would like to thank Chun-Yang Wang, Jing Wang, Zhen-Hui Sun, Xiu-Ying Zhang, Qing-Hui Li and Chuan-Zheng Miao for fruitful discussions and useful comments.

**Data availability** All data generated or analyzed during this study are included in this published article.

## Declarations

**Conflict of interest** The authors have no known competing financial interests or personal relationships that could have appeared to influence the work reported in this paper.

- 
- [1] Okołowicz, J., Płoszajczak, M., Rotter, I.: Dynamics of quantum systems embedded in a continuum. *Phys. Rep.* **374**, 271-383 (2003).
  - [2] Pauli, W.: On Dirac's New Method of Field Quantization. *Rev. Mod. Phys.* **15**, 175-207 (1943).
  - [3] Dirac, P.A.M.: Bakerian Lecture - The physical interpretation of quantum mechanics. *Proc. R. Soc. London Ser. A-Math. Phys. Eng. Sci.* **180**, 1-40 (1942).
  - [4] Lee, T.D., Wick, G.C.: Negative metric and the unitarity of the S-matrix. *Nucl. Phys. B* **9**, 209-243 (1969).
  - [5] Brower, R.C., Furman, M.A., Moshe, M.: Critical exponents for the Reggeon quantum spin model. *Phys. Lett. B* **76**, 213-219 (1978).
  - [6] Benjamin, C.H., Stanley, T.J., Tan, C.I.: Complex energy spectra in reggeon quantum mechanics with quartic interactions. *Nucl. Phys. B* **171**, 392-412 (1980).
  - [7] Benjamin, C.H., Stanley, T.J., Tan, C.I.: New structure in the energy spectrum of reggeon quantum mechanics with quartic couplings. *Phys. Lett. B* **91**, 291-295 (1980).
  - [8] Caliceti, E., Graffi, S., Maioli, M.: Perturbation Theory of Odd Anharmonic Oscillators. *Commun. Math. Phys.* **75**, 51-66 (1980).

- [9] Scholtz, F.G., Geyer, H.B., Hahne, F.J.W.: Quasi-Hermitian operators in quantum mechanics and the variational principle. *Ann. Phys.* **213**, 74-101 (1992).
- [10] Bender, C.M., Boettcher, S.: Real Spectra in Non-Hermitian Hamiltonians Having  $\mathcal{PT}$  Symmetry. *Phys. Rev. Lett.* **80**, 5243-5246 (1998).
- [11] Okuma, N., Kawabata, K., Shiozaki, K., Sato, M.: Topological Origin of Non-Hermitian Skin Effects. *Phys. Rev. Lett.* **124**, 086801 (2020).
- [12] Yang, Z., Zhang, K., Fang, C., Hu, J.: Non-Hermitian Bulk-Boundary Correspondence and Auxiliary Generalized Brillouin Zone Theory. *Phys. Rev. Lett.* **125**, 226402 (2020).
- [13] Zhang, K., Yang, Z., Fang, C.: Correspondence between Winding Numbers and Skin Modes in Non-Hermitian Systems. *Phys. Rev. Lett.* **125**, 126402 (2020).
- [14] Hamazaki, R., Kawabata, K., Kura, N., Ueda, M.: Universality classes of non-Hermitian random matrices. *Phys. Rev. Res.* **2**, 023286 (2020).
- [15] Wang, X.R., Guo, C.X., Du, Q., Kou, S.P.: State-Dependent Topological Invariants and Anomalous Bulk-Boundary Correspondence in Non-Hermitian Topological Systems with Generalized Inversion Symmetry. *Chin. Phys. Lett.* **37**, 117303 (2020).
- [16] Li, T., Zhang, Y.S., Yi, W.: Two-Dimensional Quantum Walk with Non-Hermitian Skin Effects. *Chin. Phys. Lett.* **38**, 030301 (2021).
- [17] Lenke, L., Mühlhauser, M., Schmidt, K.P.: High-order series expansion of non-Hermitian quantum spin models. *Phys. Rev. B* **104**, 195137 (2021).
- [18] Guo, A., Salamo, G.J., Christodoulides, D.N., et al.: Observation of  $\mathcal{PT}$ -symmetry breaking in complex optical potentials. *Phys. Rev. Lett.* **103**, 093902 (2009).
- [19] Chou, T., Mallick, K., Zia, R.K.P.: Non-equilibrium statistical mechanics: from a paradigmatic model to biological transport. *Rep. Prog. Phys.* **74**, 116601 (2011).
- [20] Bertoldi, K., Vitelli, V., Christensen, J., Martin van, H.: Flexible mechanical metamaterials. *Nat. Rev. Mater.* **2**, 17066 (2017).
- [21] Weimann, S., Kremer, M., Plotnik, Y., Lumer, Y., Nolte, S., Makris, K.G., Segev, M., Rechtsman, M.C., Szameit, A.: Topologically protected bound states in photonic parity-time-symmetric crystals. *Nat. Mater.* **16**, 433-438 (2017).
- [22] Longhi, S.: Parity-time symmetry meets photonics: A new twist in non-Hermitian optics. *Europhys. Lett.* **120**, 64001 (2017).
- [23] Lebrat, M., Hausler, S., Fabritius, P., Husmann, D., Corman, L., Esslinger, T.: Quantized

- Conductance through a Spin-Selective Atomic Point Contact. *Phys. Rev. Lett.* **123**, 193605 (2019).
- [24] Yang, W., Wenquan, L., JiangFeng, D., et al.: Observation of parity-time symmetry breaking in a single-spin system. *Science* **364**, 878-880 (2019).
  - [25] Amico, L., Fazio, R., Osterloh, A., Vedral, V.: Entanglement in many-body systems. *Rev. Mod. Phys.* **80**, 517-576 (2008).
  - [26] Eisert, J., Cramer, M., Plenio, M.B.: Colloquium: Area laws for the entanglement entropy. *Rev. Mod. Phys.* **82**, 277-306 (2010).
  - [27] Nishioka, T.: Entanglement entropy: Holography and renormalization group. *Rev. Mod. Phys.* **90**, 035007 (2018).
  - [28] Kitaev, A., Preskill, J.: Topological entanglement entropy. *Phys. Rev. Lett.* **96**, 110404 (2006).
  - [29] Zhang, Y., Grover, T., Turner, A., Oshikawa, M., Vishwanath, A.: Quasiparticle statistics and braiding from ground-state entanglement. *Phys. Rev. B* **85**, 235151 (2012).
  - [30] Osterloh, A., Luigi, A., Falci, G., Rosario, F.: Scaling of entanglement close to a quantum phase transition. *Nature* **416**, 608-610 (2002).
  - [31] Hastings, M.B.: Entropy and entanglement in quantum ground states. *Phys. Rev. B* **76**, 035114 (2007).
  - [32] Jafari, R., Kargarian, M., Langari, A., Siahatgar, M.: Phase diagram and entanglement of the Ising model with Dzyaloshinskii-Moriya interaction. *Phys. Rev. B* **78**, 214414 (2008).
  - [33] Brandão, F.G.S.L., Horodecki, M.: An area law for entanglement from exponential decay of correlations. *Nat. Phys.* **9**, 721-726 (2013).
  - [34] Srednicki, M.: Entropy and area. *Phys. Rev. Lett.* **71**, 666-669 (1993).
  - [35] Ryu, S., Takayanagi, T.: Holographic derivation of entanglement entropy from the anti-de Sitter space/conformal field theory correspondence. *Phys. Rev. Lett.* **96**, 181602 (2006).
  - [36] Nicola, S.D., Michailidis, A.A., Serbyn, M.: Entanglement View of Dynamical Quantum Phase Transitions. *Phys. Rev. Lett.* **126**, 040602 (2021).
  - [37] Modak, R., Mandal, B.P.: Eigenstate entanglement entropy in a  $\mathcal{PT}$ -invariant non-Hermitian system. *Phys. Rev. A* **103**, 062416 (2021).
  - [38] Arnesen, M.C., Bose, S., Vedral, V.: Natural thermal and magnetic entanglement in the 1D Heisenberg model. *Phys. Rev. Lett.* **87**, 017901 (2001).
  - [39] Kargarian, M., Jafari, R., Langari, A.: Dzyaloshinskii-Moriya interaction and anisotropy

- effects on the entanglement of the Heisenberg model. *Phys. Rev. A* **79**, 042319 (2009).
- [40] Ma, F.W., Liu, S.X., Kong, X.M.: Quantum entanglement and quantum phase transition in the XY model with staggered Dzyaloshinskii-Moriya interaction. *Phys. Rev. A* **84**, 042302 (2011).
- [41] Mehran, E., Mahdavifar, S., Jafari, R.: Induced effects of the Dzyaloshinskii-Moriya interaction on the thermal entanglement in spin-1/2 Heisenberg chains. *Phys. Rev. A* **89**, 042306 (2014).
- [42] Zhang, P.P., Wang, J., Xu, Y.L., Wang, C.Y., Kong, X.M.: Quantum Entanglements in mixed-spin XY systems. *Physica A* **566**, 125643 (2021).
- [43] Wang, Z., Fang, P.P., Xu, Y.L., Wang, C.Y., Zhang, R.T., Zhang, H., Kong, X.M.: Quantum quench dynamics in XY spin chain with ferromagnetic and antiferromagnetic interactions. *Physica A* **581**, 126205 (2021).
- [44] Walborn, S.P., Souto, R.P.H., Davidovich, L., Mintert, F., Buchleitner, A.: Experimental determination of entanglement with a single measurement. *Nature* **440**, 1022-1024 (2006).
- [45] Adam, M.K., Tai, M.E., Alexander, L., Matthew, R., Robert, S., Philipp, M.P., Greiner, M.: Quantum thermalization through entanglement in an isolated many-body system. *Science* **353**, 794-800 (2016).
- [46] Chang, P.Y., You, J.S., Wen, X., Ryu, S.: Entanglement spectrum and entropy in topological non-Hermitian systems and nonunitary conformal field theory. *Phys. Rev. Res.* **2**, 033069 (2020).
- [47] Herviou, L., Regnault, N., Bardarson, J.H.: Entanglement spectrum and symmetries in non-Hermitian fermionic non-interacting models. *SciPost Phys.* **7**, 069 (2019).
- [48] Lee, E., Lee, H., Yang, B.J.: Many-body approach to non-Hermitian physics in fermionic systems. *Phys. Rev. B* **101**, 121109 (2020).
- [49] Bácsi, Á., Dóra, B.: Dynamics of entanglement after exceptional quantum quench. *Phys. Rev. B* **103**, 085137 (2021).
- [50] Jian, S.K., Yang, Z.C., Bi, Z., Chen, X.: Yang-Lee edge singularity triggered entanglement transition. *Phys. Rev. B* **104**, L161107 (2021).
- [51] Lakkaraju, L.G.C., Sen, A.: Detection of an unbroken phase of a non-Hermitian system via a Hermitian factorization surface. *Phys. Rev. A* **104**, 052222 (2021).
- [52] Sadhukhan, D., Prabhu, R., Sen, D.A., Sen, U.: Quantum correlations in quenched disordered



- spin models: Enhanced order from disorder by thermal fluctuations. Phys. Rev. E **93**, 032115 (2016).
- [53] Jafari, R., Akbari, A.: Dynamics of quantum coherence and quantum Fisher information after a sudden quench. Phys. Rev. A **101**, 062105 (2020).
  - [54] Fel'dman, E.B., Rudavets, M.G.: Exact results on spin dynamics and multiple quantum NMR dynamics in alternating spin-1/2 chains with XY Hamiltonian at high temperatures. JETP Lett. **81**, 47-52 (2005).
  - [55] Kuznetsova, E.I., Fel'dman, É.B.: Exact solutions in the dynamics of alternating open chains of spins  $s = 1/2$  with the XY Hamiltonian and their application to problems of multiple-quantum dynamics and quantum information theory. J. Exp. Theor. Phys. **102**, 882-893 (2006).
  - [56] Giorgi, G.L.: Ground-state factorization and quantum phase transition in dimerized spin chains. Phys. Rev. B **79**, 060405 (2009).
  - [57] Giorgi, G.L.: Spontaneous  $\mathcal{PT}$  symmetry breaking and quantum phase transitions in dimerized spin chains. Phys. Rev. B **82**, 052404 (2010).
  - [58] Wootters, W.K.: Entanglement of Formation of an Arbitrary State of Two Qubits. Phys. Rev. Lett. **80**, 2245-2248 (1998).
  - [59] Ashida, Y., Furukawa, S., Ueda, M.: Parity-time-symmetric quantum critical phenomena. Nat. Commun. **8**, 15791 (2017).
  - [60] Sternheim, M.M., Walker, J.F.: Non-Hermitian Hamiltonians, Decaying States, and Perturbation Theory. Phys. Rev. C **6**, 114-121 (1972).
  - [61] Brody, D.C.: Biorthogonal quantum mechanics. J. Phys. A-Math. Theor. **47**, 035305 (2014).
  - [62] Sousa, J.R.d., Albuquerque, D.F.d., Fittipaldi, I.P.: Tricritical behavior of a Heisenberg model with Dzyaloshinski-Moriya interaction. Phys. Lett. A **191**, 275-278 (1994).
  - [63] Ricardo, d.S.J., Lacerda, F., Fittipaldi, I.P.: Thermal behavior of a Heisenberg model with DM interaction. J. Magn. Magn. Mater. **140-144**, 1501-1502 (1995).